This manuscript was published as formal in:

CARBOHYDRATE POLYMERS Volume: 179 Pages: 59-70 Published: JAN 1 2018

https://doi.org/10.1016/j.carbpol.2017.09.066

https://www.sciencedirect.com/science/article/pii/S0144861717310998

Title:

Biocompatible chitosan based hydrogels for potential application in local tumour therapy

by:

Anda-Mihaela Olaru[1,2], Luminita Marin[1]*, Simona Morariu[1], Gabriela Pricope[1], Mariana Pinteala[1], Liliana Tartau-Mititelu[3]

[1] "Petru Poni" Institute of Macromolecular Chemistry of Romanian Academy, Iasi, Romania

[2] "Alexandru Ioan Cuza" University, Department of Organic Chemistry, Iasi, Romania

[3] "Gr .T. Popa" University of Medicine and Pharmacy, Iasi, Romania

*Corresponding author e-mail: lmarin@icmpp.ro

*Corresponding Author Luminita Marin

e-mail: lmarin@icmpp.ro

Abstract

A series of hydrogels based on chitosan polyamine and nitrosalicylaldehyde were prepared *via* dynamic covalent chemistry (DCC), by imination and transimination reactions towards ordered clusters which play the role of crosslinking nodes of the chitosan network. The hydrogelation mechanism has been proved through NMR and FTIR spectroscopy, X-ray diffraction and polarized light microscopy. The successful preparation of the hydrogels and their mechanical properties were further investigated using rheological measurements. By electron scanning microscopy, the hydrogels exhibited a channels microstructure morphology which critically influenced their fast swelling by capillarity. The hydrogels cytotoxicity was explored *in vitro* on HeLa cancer cells and their biocompatibility was monitored *in vivo* by subcutaneous implantation on rats. The novel hydrogels proved good *in vitro* cytotoxicity on the HeLa cells and also *in vivo* biocompatibility in rats. Thus, these novel biomaterials promise to be suitable for local cancer therapy.

KEYWORDS: chitosan, nitrosalicylaldehyde, hydrogel, biocompatibility, antitumor

1. INTRODUCTION

Hydrogels are a class of soft materials extensively employed in industrial and biomedical applications. Due to their high content of water and mechanical properties similar to the natural tissues – biocompatible hydrogels are at the forefront of materials designed for tissue engineering or drug carriers. One attractive direction of their bio-application is that of precision medicine and local therapy, in particular in the cancer therapy when injection at the tumour site minimizes the side effects (Ta, Dass & Dunstan, 2008; Hong, Yoo, Kim, & Lee, 2017; Sedghi et al., 2017). To this aim, hydrogels which allow an easy formulation to control the gelling time are desirable. Besides, multifunctional hydrogels which respond under the environmental stimuli as pH or temperature are further of interest in the local treatments or tissue engineering. Recent papers on this subject reported outstanding achievements. For instance, hydrogels based on PEG were successfully implemented for the treatment of heart attacks (Johnson et al., 2015), as sealants for the treatment of severe haemorrhage (Konieczynska et al., 2017) or adhesives easily removable for the treatment of second-degree burn wounds (Konieczynska et al., 2016). Chitosan based hydrogels provided good results as promoters of wound healing (Sandri et al., 2017), treatment of focal infections caused by antibiotic resistant bacteria (Korupalli et al., 2017), in loco-regional treatment of hepatocellular carcinoma (Salis et al., 2015), in photodynamic cancer therapy (Ferreiraa et al., 2016) or in stem cell therapy (Naderi-Meshkin et al., 2016). It was established that the

supramolecular architecture of the hydrogels is of critical impact in regenerative medicine, having the ability to control cell behaviour in cell therapy (Storrie et al., 2007; Latxague et al., 2015).

Chitosan is an important component of the hydrogels applied in tissue engineering and drug delivery, due to its intrinsic biocompatibility, biodegradability, bioadhesivity, antimicrobial and haemostatic properties. Its ability to accelerate wound healing by modulating the function of the inflammatory cells is further of interest in the local therapy (Sandri et al., 2017). Due to its polycationic nature, its gelling is favoured by the basic pH (Montembault, Viton, & Domard, 2005), an important advantage in limiting the local spreading of the chitosan gel precursors in tumours or infected tissues with local acidosis (Zhang, Lin, & Gillies, 2010; Punnia-Moorthy, 1987). The main issue in using chitosan hydrogels is related to the crosslinker – generally a dialdehyde, usually glutaraldehyde, – recently proved to have a degree of toxicity to the human body (Beauchamp, St Clair, Fennell, Clarke, & Morgan, 1992).

The research work of our group revealed a new concept of crosslinking of chitosan polyamine with monoaldehydes based on the reversible condensation toward imine units, which further self-order to form clusters which play the role of chitosan crosslinkers (Marin, Simionescu, & Barboiu, 2012; Marin et al., 2014; Ailincai et al., 2016; Marin, Ailincai, Morariu, & Tartau-Mititelu, 2017; Iftime, Morariu, & Marin, 2017). The self-order ability of the newly formed imine units is favoured by the imination and transimination reactions on the chitosan polyamine under the pressure of reaching the most stable structures, by dynamic covalent chemistry (DCC) (Liu, & Li, 2013; Ruff et al., 2010; Nasr et al., 2009; Marin et al., 2016). The method is advantageous, due to the large variety of safe aldehydes and their safer use compared to the dialdehydes (Beauchamp, St Clair, Fennell, Clarke, & Morgan, 1992) which allow the tuning of the hydrogel properties.

In this context, we designed hydrogels based on chitosan and nitrosalicylaldehyde for local targeting of tumours. The rational design took into consideration the antitumor effect proved by chitosan (Mattaveewonga et al., 2016; Xia, Liu, Zhang, & Chen, 2011) and by the imines based on nitrosalicyladehyde residue (Luo, Sui, Lin, & Wu, 2016; Lu, Guo, Sang, & Guo, 2013; Zahedifard et al., 2015; Rama, & Selvameena, 2015). It was reported that imines bearing nitrosalicylaldehyde residue have significantly improved antitumor activity compared to other substituents, e.g. halogen derivatives (Luo, Sui, Lin, & Wu, 2016). It was envisioned that combining chitosan with nitrosalicylaldehyde will produce supramolecular hydrogels *via* DCC pathway. They keep good premises to combine the beneficial properties of chitosan in

protecting the tissues with the antitumor activity of the nitrosalicylaldehyde, with a local spreading of the hydrogels limited by the basic pH of the normal tissue. As a proof of concept, supramolecular hydrogels were obtained from chitosan and nitrosalicylaldehyde, with a fast gelling in contact with a basic medium and self-healing in an acidic medium, with good *in vitro* cytotoxicity on HeLa tumor cell line and *in vivo* biocompatibility on rats.

2. EXPERIMENTAL

2.1.Materials

2-hydroxy-5-nitrobenzaldehyde (nitrosalicylaldehyde) (98%), chitosan (217.74 kDa, DA: 85 %), D-glucosamine hydrochloride, phosphate buffer (1.0 M, pH=7.4) were purchased from Aldrich and used as received. Buffer solution pH=4±0.02 was purchased from Carl Roth. HeLa cells (from CLS-Cell-Lines-Services-GmbH, Germany) were cultivated in tissue culture flasks with alpha-MEM medium (Lonza) supplemented with 10% fetal bovine serum (FBS, Biochrom GmbH, Germany) and 1% Penicillin-Streptomycin-Amphotericin B mixture (10K/10K/25 µg in 100 ml, Lonza). The medium was changed with fresh one every 3 or 4 days. Once cells have reached confluency, they were detached with 1x Trypsin-Versene (EDTA) mixture (Lonza), washed with phosphate buffered saline (PBS, Invitrogen), centrifuged at 200 x g for 3 minutes and subcultured into new tissue culture flasks.

2.2.Syntheses

Model compound (**MC**):

A model compound was synthetized from 2-hydroxy-5-nitrobenzaldehyde (5-nitrosalicylaldehyde) and glucosamine (Scheme 1) in order to obtain a characterization data set to properly confirm the synthetic pathway and to better understand the studied properties.

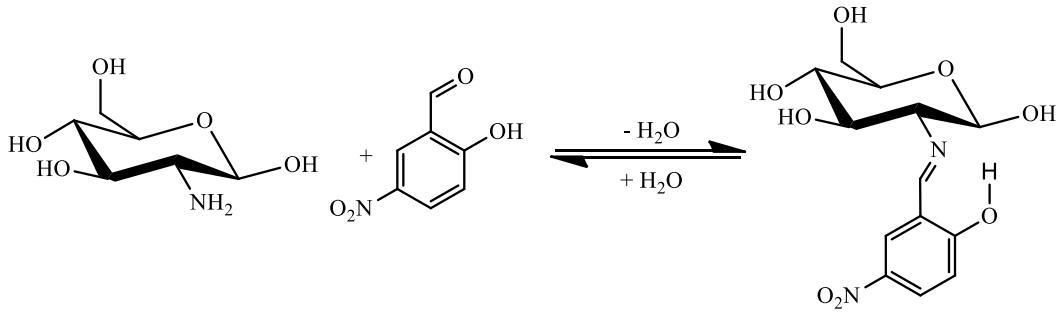

Scheme 1. Synthesis of the model compound (**MC**)

A solution of D-glucosamine hydrochloride (0.1 g, 0.464 mmol) in water (1.2 mL) was heated at 35 ºC and then loaded to an anion exchanger column (Amberlite IRA-67 resin). The free glucosamine solution was allowed to slowly drop wise to the 6% nitrosalicylaldehyde solution

(0.033g, 0.197 mmol) in ethanol, under vigorous magnetic stirring, at 35 ^{o}C. After 4 h a yellow solid precipitated. The yellow powder was filtered, washed with a mixture of water and ethanol (2/1; v/v) and recrystallized from acetonitrile to give yellow needles proper for single crystal X-ray analysis, 74% yield. $C_{13}H_{16}N_2O_7$: M_r = 312 g mol^{-1}; space Group: I2; cell lengths: a = 10.127(6) Å, b = 5.155(5) Å, c = 27.746(8) Å; cell angles: α = 90 ^{o}, β = 93.04(4) ^{o}, γ = 90 ^{o}; cell volume: V = 1446.43 Å^3.; FTIR (KBr): 1613 ($\nu_{CH=N}$), 1546 ($\nu_{C=C}$), 1510 (ν_{NO2} asym), 1321 (ν_{NO2} sym), 1236 (ν_{OH}).; ^{1}H NMR (400.13 MHz, DMSO-d$_6$, ppm): δ = 8.71 (s, 1H, C<u>H</u>=N), 8.54 and 8.49 (s, 1H$_{ar}$ α/β=5.6/1), 8.14, 8.12 and 8.05, 8.03 (d, 1H, α/β=5.6/1), 7.18, 7.17 and 7.09, 7.08 (d, 1H, -O<u>H</u>, α/β=5.6/1), 6.82, 6.8 and 6.6, 6.57 (d, 1Har α/β=5.6/1), 5.57, 5,54 and 5.44, 5.42 (d, 1H, -O<u>H</u>, α/β=5.6/1), 5.24, 5.20 and 5.18, 5.17 (d, 1H, -O<u>H</u>, α/β=5.6/1), 4.85, 4.83, 4.81 and 4.59, 4.57, 4.55 (t, 1H, α/β=5.6/1), 4.64 and 4.57 (s, 1H, -O<u>H</u>, α/β=5.6/1), 3.74-3.16 (superposed peaks, 4H), 3.09, 3.07, 3.05(t, 1H).

Hydrogels: The hydrogels synthesis has been performed according to a published procedure (Marin, Ailincai, Morariu, & Tartau-Mititelu, 2017; Iftime, Morariu, & Marin, 2017). Shortly, a 1% solution of nitrosalicylaldehyde in ethanol has been slowly dropped under vigorous stirring into a round bottom flask containing a solution of 2% chitosan in 0.7% acetic acid at 55 ^{o}C. The amounts of aldehyde and chitosan were calculated to correspond to different molar ratios of the glucosamine units of chitosan to aldehyde, from 1/1 to 10/1 (Table 1). The gelation of the reaction mixture occurred at different times, depending on the molar ratio of the functional groups (Table 1). The gels were semisolid, transparent, deep yellow materials, with orange luminescence under UV lamp. Their NMR spectra confirmed the total conversion of the aldehyde into imine linkages. The hydrogels were kept around 48 hours to remove the ethanol, and further they were lyophilized to obtain the corresponding xerogels.

Table 1. Reaction parameters of the hydrogel synthesis

Code	**A1**	**A2**	**A3**	**A4**	**A4.5**	**A5**	**A5.5**	**A6**	**A7**	**A8.5**	**A10**
NH_2:CHO ratio	1:1	2:1	3:1	4:1	4.5:1	5:1	5.5:1	6:1	7:1	8.5:1	10:1
Chitosan (mg)	60	60	60	60	60	60	60	60	60	60	60
NSA (mg)	51.6	25.8	17.0	12.9	11.5	10.4	9.4	8.5	7.4	6.1	5.2
Gelation time (min)	*	*	*	*	*	1	60	120	1440	-	-
Xerogels (mg)	111.6	85.8	77.0	72.9	71.5	70.4	69.4	68.5	67.4	66.1	65.2

*The gelation occurred instantaneous as the aldehyde solution was added; NSA= 2-hydroxy-5-nitrobenzaldehyde (nitrosalicylaldehyde)

2.3. Equipment and measurements

The *NMR spectra* were registered with a BRUKER Avance DRX 400 MHz spectrometer, at room temperature. The chemical shifts were reported as δ values (ppm) relative to the residual peak of the deuterated solvent.

ATR-FTIR spectra of the model compound, chitosan and the chitosan based hydrogels were measured on a FT-IR Bruker Vertex 70 Spectrofotometer. The spectra were processed using OPUS 6.5 software.

X-Ray Diffraction of the xerogels was performed by wide angle technique (WAXD) on a Bruker D8 Avance diffractometer, using Ni-filtered Cu-Kα radiation (λ = 0.1541 nm), working conditions: 36 kV, 30 mA. The diffractograms were recorded in the 2÷50^o range ($2\theta°$), at room temperature. The samples were prepared as pellets by applying a pressure of 10 N/m^2. X-ray diffraction of the model compound has been performed by single crystal X-ray diffraction techniques on an Oxford-Diffraction XCALIBUR E CCD diffractometer equipped with graphite-monochromated Mo Kα radiation.

Polarized light microscopy (POM) of the model compound and hydrogels was performed with an Olympus BH-2 polarized light microscope, on thin samples placed between two lamellae.

Scanning electron microscopy (SEM) was realized with a field emission Scanning Electron Microscope SEM EDAX – Quanta 200, operated at an accelerating voltage of 20 keV.

The swelling of the hydrogels was monitored by calculating the mass equilibrium swelling (MES), with the equation: MES = (Ms-Md)/Md, where Ms is the mass of the hydrogel in swollen state and Md is the mass of the hydrogel in the initial dried state. The measurements were performed on three different pieces of each xerogel. The samples were immersed in vials containing 20 mL of swelling media, and their mass was weight from time to time, until became constant. To establish the stability of the hydrogels, the samples were kept in swelling media for three months, and weighted weekly.

The *rheological properties* of the hydrogels were determined at 37 °C on a MCR302 Anton-Paar rheometer equipped with a Peltier device. All measurements were registered with a plane-plane geometry (diameter of 25 mm) and an anti-evaporation device. The following rheological tests were carried out in order to establish the viscoelastic properties of the prepared samples: a) amplitude sweep tests at 10 rad/s in the stress range of $8x10^{-3}$ Pa - $5x10^2$ Pa, which allowed the determination of the linear viscoelastic regime (LVR) for each sample; b) frequency sweep measurements at a constant shear stress value from LVR in the frequency range of 0.5 rad/s - 10^2 rad/s in order to determine the values of the storage (G') and loss (G")

moduli; c) steady flow measurements performed at shear rates between 10^{-3} 1/s and $2x10^{2}$ 1/s to establish the zero shear viscosity (η_o) and critical yield stress (τ_c) values; d) oscillatory step tests at 10 rad/s carried out alternatively for 120 s at low strain (1%) and 30 s at very high strain (1000%), only for the samples with gel-like properties which were dried by lyophilisation and then swollen in water; the samples were subjected to two pulses of high strain and the structure recovery was monitored in each case. The values of zero shear viscosity (η_o) were determined using the Cross equation (Cross, 1965):

$$\eta = \eta_\infty + (\eta_o - \eta_\infty)/(1 + (\alpha \cdot \dot{\gamma})^n) \quad (1)$$

where n is a dimensionless constant, α is a constant which can be associated with the rupture of the linkages in the material structure. η_o and η_∞ represent the viscosities at zero and infinite shear rate, respectively. For fitting of experimental data with eq. 1, it was considered η_∞ as being the viscosity of water at 37 °C (0.690 mPa·s) because our data did not reach the Newtonian region.

In vitro cytotoxicity study: The *in vitro* cytotoxicity has been evaluated by direct contact method, following ISO standard 10993-5 (Wang et al., 2013). Prior to the tests, the hydrogels were sterilized by immersion in 70% ethanol solution, washed twice in sterile ultrapure water, air dried in a sterile environment and kept under UV for 30 minutes (Dai et all., 2016). The aldehyde precursor (NSA), the model compound (MC) and the chitosan (C) used as control references were sterilized only by UV exposure. Cytotoxicity was measured using the CellTiter 96® Aqueous One Solution Cell Proliferation Assay (Promega). HeLa cells were seeded into a 96-well culture plate at a density of $1x10^4$ cells per well in 100 µl culture medium (alpha-MEM medium supplemented with 10% fetal bovine serum (FBS) and 1% Penicillin-Streptomycin-Amphotericin B mixture (10K/10K/25 µg)). After 24 hours the medium in each well was replaced with 200 µl mixture containing fresh medium and solution of model compound or aldehyde. For direct hydrogel-cell contact various amounts of hydrogel, 6.46 mg **A2** containing 0.318 µmol imine units; 7.2 mg **A3** containing 0.241 µmol imine units, and 7.6 mg **A4** containing 0.190 µmol imine units, were placed to each well containing 200 µl cell culture medium. The activity of the aldehyde precursor and model compound was screened for 1% DMSO solutions containing similar amounts to those comprised in the tested hydrogels, meaning 0.054 mg (**NSA**2), 0.04 mg (**NSA**3), 0.034 mg (**NSA**4) in the case of the aldehyde and of 0.104 mg (**MC**2), 0.079 mg (**MC**3), 0.064 mg (**MC**4) in the case of the model compound. 8 biological replicates were performed for each sample. After 44 hours, the hydrogel was removed from each well along with 100 µl cell

medium. 20 μL of CellTiter 96® Aqueous One Solution reagent was added to each well, and the plates were incubated for another 4 hours before reading the results. Absorbance at 490 nm was recorded with a plate reader (EnSight, PerkinElmer). Cell viability was calculated and expressed as percentage relative to viability of the untreated cells which served as negative control for the hydrogels. Cells incubated with 1% DMSO served as negative control for the model compound and aldehyde. After 24 and 48 hours of incubation, all cell culture plates were inspected using an inverted microscope Leica DMI 3000 B and images were acquired using the bright field filter and the 5X objective.

In vivo biocompatibility was performed on rats by subcutaneous implantation tests (Peacman, 2011). The animals were housed in plastic cages, under standard laboratory conditions (22-24^{o}C, relative humidity 55-65% and a cycle 12-hour light/12-hour dark), with free access to water and standard diet (granulated food), except during the period of the experiments. After a quarantine period of 7 days, the rats were randomly divided into 5 groups of 6 animals each, according to the following protocol: **Group I (C):** control group (without pellets); **Group II (C-p):** positive control group (with cotton pellets implantation); **Group III (A2): A2** hydrogel; **Group IV (A3): A3** hydrogel; **Group V (A4): A4** hydrogel. For the *in vivo* biocompatibility of these hydrogels, after subcutaneous implantation in rats, the standardized granuloma model was performed. In positive control group rats, sterile cotton pellets saturated with saline solution were used. A control group without implanted pellets were used as negative control reference (**C**).

At the beginning of the experiment, animals were anaesthetized with ketamine and xylazine, incised in one side in their dorsal area and pellets of 62 mg (with cotton or with different hydrogels) were subcutaneous introduced. The implanted pellets reacted as a foreign constituent, inducing a subacute local inflammatory reaction. The implanted hydrogels were obtained from 0.9 mg of chitosan and different amounts of aldehyde: 0.4 mg for **A2**, 0.27 mg for **A3** and 0.209 for **A4**.

The biocompatibility properties of the hydrogels were studied by assessing the effects on the blood, the serum biochemical and immune parameters. After 24 hours of the experiment and after 8 days, 0.5 ml of blood samples were taken from the ophthalmic vein of rats anaesthetized with ethylic ether, and the following parameters were determined: the differential white cell percentage (polymorphonuclear neutrophils - PMN, lymphocytes - Ly, eosinophils - E, monocytes - M, basophils - B). In addition, the liver enzymes (glutamic pyruvic transaminase – GPT, glutamic oxaloacetic transaminase – GOT and lactic

dehydrogenase - LDH) activity was examined (De Jong, Carraway, & Geertsma, 2012; Wolf, & Andwraon, 2012).

In the eighth day of the investigation, the phagocytic capacity of peripheral neutrophils (the nitro-blue tetrazolium - NBT test) and the activity of serum complement were assessed. These parameters belong from a group of tests used to monitor the immunologic effects of the pharmacologic agents in experimental studies on laboratory animals (Peacman, 2011).

Data were analysed using SPSS 17.0 for Windows program; the one-way ANOVA method was used to compare the mean values of the groups; the two-way ANOVA and the Newman-Keuls post-hoc method were used for multiple comparisons of the mean values. The differences having the P-value below 0.05 were considered to be significant comparing to control group. Experimental protocol was implemented according to recommendations of the ``Grigore T. Popa`` University Committee for Research and Ethical Issues in agreement with the international guidelines, for handling and use of experimental animals. Each rat was used once only, and the interval of the experiments was kept as short as possible. For ethical reasons, all the animals were sacrificed at the finalization of the study (Protocole, 1998).

3. RESULTS AND DISCUSSIONS

3.1.Synthesis and characterization. Imine formation and its stability

Supramolecular hydrogels were prepared by reacting chitosan with 2-hydroxy-5-nitrobenzaldehyde (nitrosalicylaldehyde) by condensation reaction assisted by the supramolecular ordering of the newly formed nitrosalicylimine-chitosan into ordered clusters, which played the role of crosslinking nodes (Marin, Ailincai, Morariu, & Tartau-Mititelu, 2017; Iftime, Morariu, & Marin, 2017). Varying the molar ratio of the NH_2/CHO functional groups, a series of hydrogels with different percentage of crosslinking nodes have been obtained, called **A1**-**A7** (Table 1). The gelation process was visually confirmed by the inversion test (Scheme 2). To better understand the gelation mechanism, a model compound (**MC**) has been synthesised from 2-hydroxy-5-nitrobenzaldehyde and glucosamine (Scheme 1). The mechanism of gelation was deciphered analysing the data of the NMR and FTIR spectroscopy and X-ray diffraction and POM images of the hydrogels and the model compound, as well.

Scheme 2. Synthesis of the hydrogels

NMR spectra revealed the formation of the imine linkage by the appearance of the characteristic chemical shift around 8.7 ppm, while the band specific to the aldehyde unit (10.3 ppm) completely disappeared indicating its total consumption (Figure 1a). Except the aromatic proton having nitro and imine ortho neighbours, the other aromatic protons and the imine proton were downfield with respect to their counterparts in the model compound, due to the intramolecular H-bonding, (Figure 1a) which reduced the valence electron density creating a deshielding effect of the molecule's edge. The slight upfield of the aromatic proton having nitro and imine ortho neighbours with respect to its counterparts in the model compound was associated with a slightly shielding effect exerted by the chitosan surrounding. Comparing with the model compound, the proton signals of the nitrosalicyl-imine segments in hydrogels were drastically broadened, feature attributed to the reducing of their mobility by grafting on the semiflexible chitosan chains (Ruff et al., 2010). Compared to other imino-chitosan derivatives (Marin, Simionescu, & Barboiu, 2012; Marin et al., 2014; Ailincai et al., 2016; Marin, Ailincai, Morariu, & Tartau-Mititelu, 2017; Iftime, Morariu, & Marin, 2017; dos Santos, Dockal, & Cavalheiro, 2005; Stroescu et al., 2015; Pestova et al., 2016) it must be noted the total conversion of the aldehyde into imine units in aqueous medium. The total shifting of the condensation equilibrium to the products was assessed to the stabilization of imine linkages (electron donor) by strong conjugation with nitro group (electron withdrawing). Besides, the imine linkages were further stabilized by intramolecular H-bond (Nasr et al., 2009; Kovaricek, & Lehn, 2012). Moreover, the poor solubility of the nitrosalicylaldehyde in water also played an important role in the shifting the equilibrium to the products (Godoy-Alcántar, Yatsimirsky, & Lehn, 2005).

To investigate the nitrosalicyl-imine stability and implicitly its ability to undergo constitutional exchange, the NMR spectrum of the model compound was registered in different conditions, at each 24 hours, during 5 consecutive days. In the ^{1}H-NMR spectrum registered in a mixture of DMSO-d6/water (20/1, v/v), the chemical shift of the aldehyde

proton appeared as a low intensity band, indicating that the aqueous medium slightly shifted the reaction equilibrium to the reagents (Supporting Information, Figure S1a). In a mixture of DMSO-d6/acetic acid 0.7% (20/1, v/v), the ^{1}H-NMR spectrum exhibited the chemical shifts of both aldehyde and amine reagents, but an insignificant signal of the imine proton, indicating that the reaction equilibrium was shifted to the reagents (Supporting Information, Figure S1b). On the contrary, as stated above, the hydrogels obtained in 0.7% solution of acetic acid showed the total shifting of the reaction equilibrium to the imine products. This fact suggests supplementary stabilization forces. It was assumed that the ability of the imine units to bond small amount of water/acetic acid inside the ordered clusters (see single crystal on the model compound) favoured the internal self-transimination processes to the most stable supramolecular architecture, increasing their strength (Kovaricek, & Lehn, 2012).

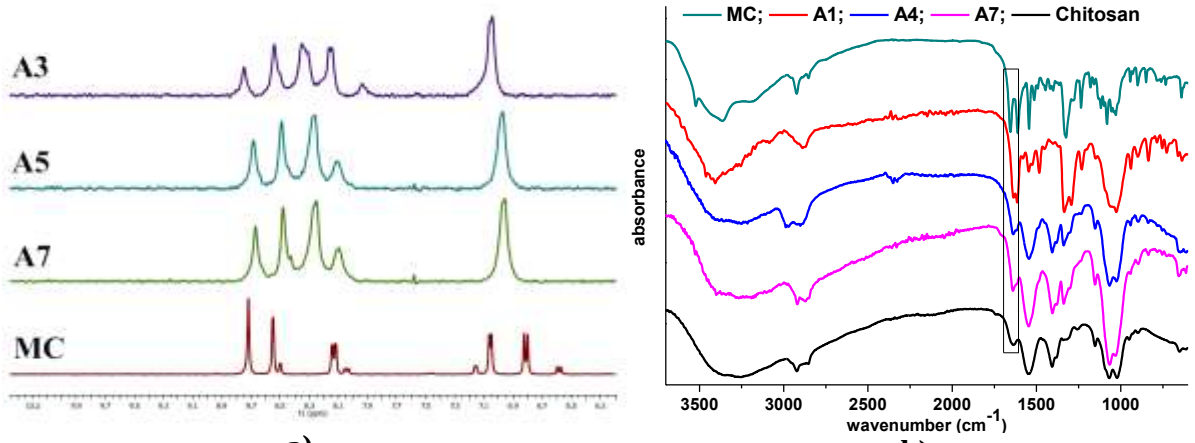

Figure 1. Comparative a) ^{1}H-NMR and b) FTIR spectra of the model compound (**MC)**, representative hydrogels and chitosan

Further, the presence of the imine band in hydrogels has been confirmed by the FTIR spectra, by the occurrence of the stretching vibration of the imine linkage (1613 cm^{-1}) as a sharp band which replaced the broad amide band of chitosan (1640 cm $^{-1}$). The imine band became much intense once the amount of aldehyde reagent increased, consistent with the increasing of the density of imine units (Figure 1b). Concomitantly, the characteristic band of the amine groups (1546 cm^{-1}) diminished indicating its consumption. Important changes in the spectral domain related to the O-H stretching vibrations, intra- and inter-molecular H-bonded (3500-2800 cm^{-1}) indicated rearrangements of the hydrogen bonding network during the gelation process, in agreement with significant modifications at supramolecular level (Marin et al., 2014; Ailincai et al., 2016; Marin, Ailincai, Morariu, & Tartau-Mititelu, 2017; Iftime, Morariu, & Marin, 2017; Marin et al., 2015).

3.2.Supramolecular architecture

The morphological changes indicated by the FTIR spectra, were clearly attributed by wide angle X-ray diffraction (WXRD) on the corresponding xerogels, which indicated modifications of the position and intensity of the reflections bands compared to chitosan, consistent with the formation of a 3D lattice (Figure 2b) (Marin et al., 2014; Ailincai et al., 2016; Marin, Ailincai, Morariu, & Tartau-Mititelu, 2017; Iftime, Morariu, & Marin, 2017; Marin et al., 2015). The 3D-architecture, as indicated by WXRD pattern, agreed well with the supramolecular architecture of the model compound (Figure 2a), indicating similar driving force for ordering. The diffraction pattern of the xerogels changed its shape compared to the chitosan one, along with increasing the density of imine units. Chitosan presented two broad reflections of low intensity, centred at 12 ^{o} (7.7 Å) and 22 ^{o} (4.41 Å), respectively, attributed to a semicrystalline morphology (Leceta, Guerrero, Ibarburu, Dueñas, & de la Caba, 2013). As the density of imine units on the chitosan backbones increased, a significant increase of the crystallinity degree occurred, involving (i) the increase in intensity of the reflection at wide angle concurrently with its shifting to lower angles (20 ^{o}) corresponding to a higher d-spacing (4.48 Å); (ii) the increase in intensity of the reflection at middle angle and its shifting from 12 to 13 ^{o}, to lower distances (6.85 Å); (iii) the appearance of a new reflection band around 6 ^{o} (14 Å) and its increase in intensity as the imine density increased. The lower angle reflection band was attributed to the layered architecture formed due to the hydrophobic/hydrophilic segregation, as the single crystal X-ray diffraction of the model compound showed (Figure 2a). Overall, the xerogels diffractograms revealed the signature of a supramolecular 3D-arrangement. Taking into consideration the different density of imine units in hydrogels, it was assumed that 3D-ordered clusters were formed. They played the role of crosslinking nodes bonding the free chitosan chains into a network (Supporting Information, Figure S2) and leading thus to hydrogelation. Compared to other imino-chitosan systems reported in literature (Marin, Simionescu, & Barboiu, 2012; Marin et al., 2014; Ailincai et al., 2016; Marin, Ailincai, Morariu, & Tartau-Mititelu, 2017; Iftime, Morariu, & Marin, 2017; de Araújoa, Barbosa, Dockal, & Cavalheiro, 2017) it could be remarked a lower intensity of the band characteristic to the inter-layer distance, reflecting a lower magnitude of the layering. This was attributed to the fast reaction of chitosan with nitrosalicylaldehyde forming stable imine units, and thus rapid occurrence of the 3D-ordered clusters of low dimension. It is worth to remark that the single crystal of the model compound entrapped water molecules inside (Figure 2a), indicating the possibility to encapsulate small amounts of water inside the ordered clusters of the hydrogels too.

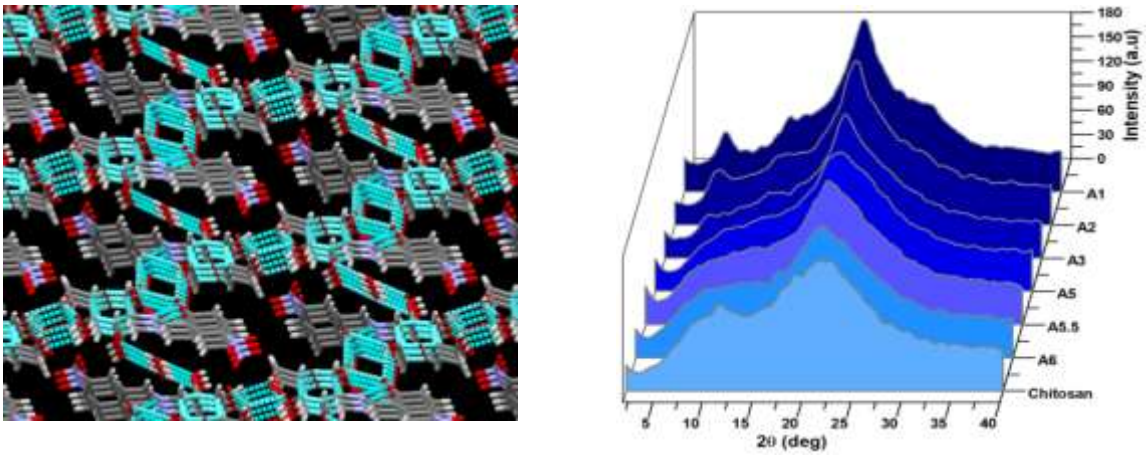

a) **b)**

c) **d)**

Figure 2. X-ray diffraction of the **a)** model compound (**MC**) on single crystal and **b)** xerogels pellets; and polarized light microscopy images of the **c)** model compound and **d)** hydrogel **A1** (the pyranose ring and the H-bonds in the crystal structure of **MC** were represented in cyan)

The supramolecular architecting of the nitrosalicylimine-chitosan was further demonstrated by polarized light microscopy (POM). As can be seen in figure 2d, the walls of the hydrogel pores were birefrigent, with a banded texture characteristic to the smectic layered mesophases of the polymer liquid crystals (Geng et al., 2003; Zabulica, Perju, Bruma, & Marin, 2014). The same banded texture could be also observed for the model compound (Figure 2c), suggesting that it originated from the layered supramolecular architecture given by segregation the nitrosalicyl-imine segments (Figure 2a). More POM microphotographs were given in Supporting Information, Figure S3.

3.3.Morphology

The morphology of the hydrogels was observed using a scanning electron microscope (SEM). They have a sponge-like aspect, with random interconnected pores of size around 50

μm forming an open channels architecture (Figure 3), which can allow a good oxygen and nutrient permeability, a good retention of the tissue fluids and a high surface-to-volume ratio - important advantages for bio-medical applications. Moreover, the interconnected pores increase the ability of a fast swelling and water retention– critical aspects for drug delivery systems or soil conditioners (Chen, Park, H., & Park, K., 1999). The pore size increased as the density of nitrosalicylimine segments in hydrogels decreased.

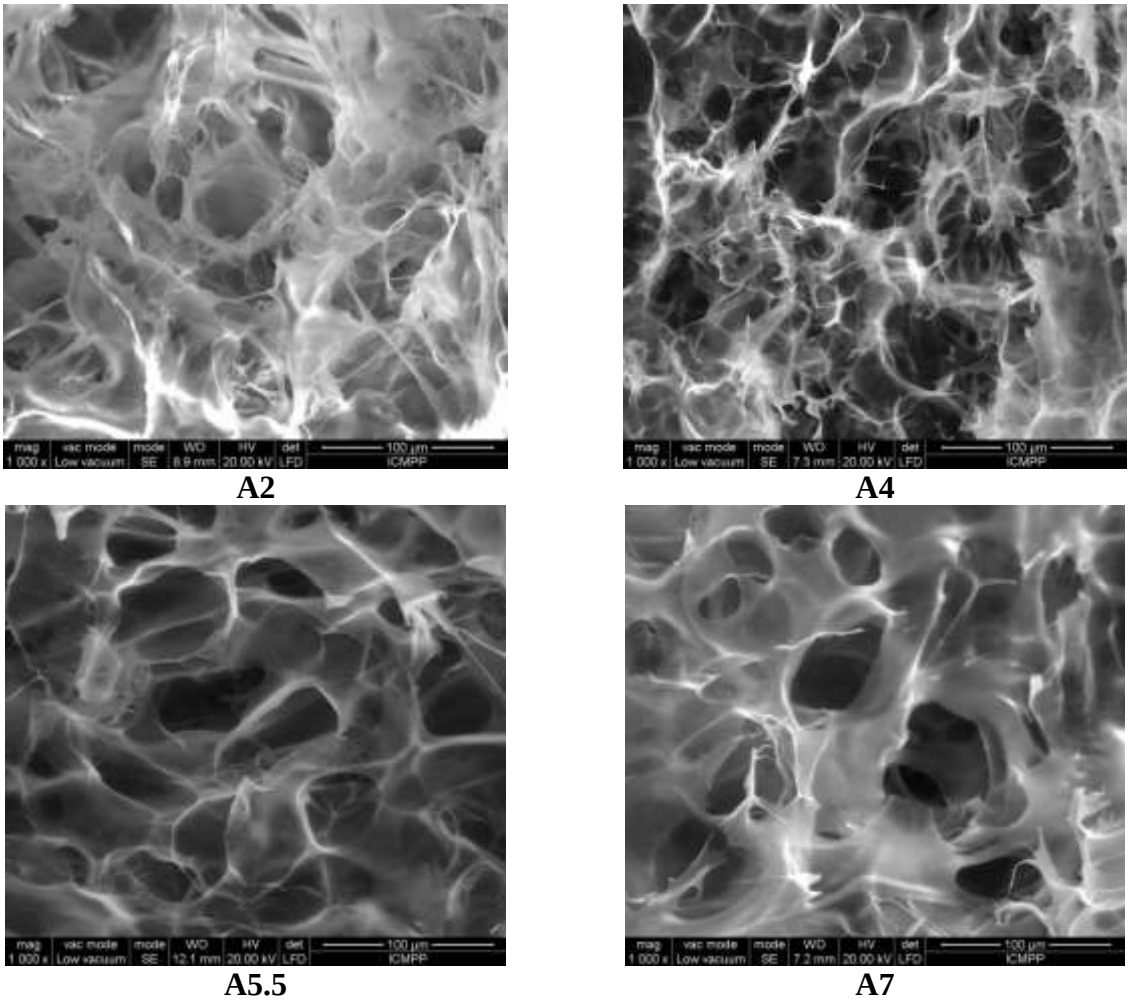

Figure 3. Representative SEM images of the xerogels

3.4. Swelling measurements

The swelling ability of the hydrogels has been investigated by measuring the mass equilibrium swelling (MES) in three media of distinct pH: (a) phosphate buffer solution (PBS) of pH = 7.4, close to that of biological tissues; (b) citrate buffer solution of pH = 4, close to the one of stomach and (c) water of neutral pH (Figure 4a), during three months.

In all three media, the hydrogels completely rehydrated and swelled very fast. The samples reached 90 %, 80 %, and 70 % of MES, in basic, acidic and neutral medium, respectively, in less than one minute (Figure 4b). Compared to the conventional hydrogels which do not swell to a measurable extent during 30 minutes, the studied hydrogels behave

similar to superporous hydrogels (Chen, Park, H., & Park, K., 1999), swelling to the equilibrium size in less than 10 minutes. This behaviour has been assigned to the channels microstructure which assured a fast swelling by capillarity. The hydrogels with higher crosslinking density (**A2**, **A3**) swelled slower, while those with medium or low crosslinking density (**A4** - **A7**) swelled faster. The MES values were close related to the pH of the swelling media and the crosslinking density of the hydrogels. It was increased when the crosslinking density decreased, reaching a maximum for **A5.5** sample. In neutral water the maximum MES had the value of 198, once again reminiscent of superporous hydrogels (Iftime, Morariu, & Marin, 2017; Chen, Park, H., & Park, K., 1999). In basic medium the hydrogels swelled less, the maximum of MES reaching the value of 47, with a good dimensional preservation (Figure 4b, c) – an important advantage for tissue engineering (El-Sherbiny, & Yacoub, 2013) or subcutaneous drug delivery (Hoare, & Kohane, 2008). Moreover, the MES slightly decreased after 5 minutes, behaviour attributed to the shrinkage of the hydrogel due to the neutralization of the traces of acetic acid in basic media. When a mixture of chitosan - nitrosalicyladehyde was injected in a phosphate buffer solution, its fast gelation has been observed, forming a spherical shape (Figure 4c). Contrary to the general behaviour of the chitosan hydrogels, in acidic medium, the MES values were lower than in water reaching the maximum value of 123 in the case of **A5.5** sample. This could be an important advantage for local administration into damaged tissues with acidic microenvironment (infected or tumours) (Zhang, Lin, & Gillies, 2010; Punnia-Moorthy, 1987). After one hour of swelling period, no significant changes of the MES were registered; the hydrogels were stable in all three media, even after 3 months. Moreover, the MES value in water still slightly increased, recommending them for agriculture applications as soil conditioners. Among the tested hydrogels that obtained for a 5.5/1 molar ratio of the $–NH_2$/-CHO functional groups proved to have the fastest swelling and the highest MES values.

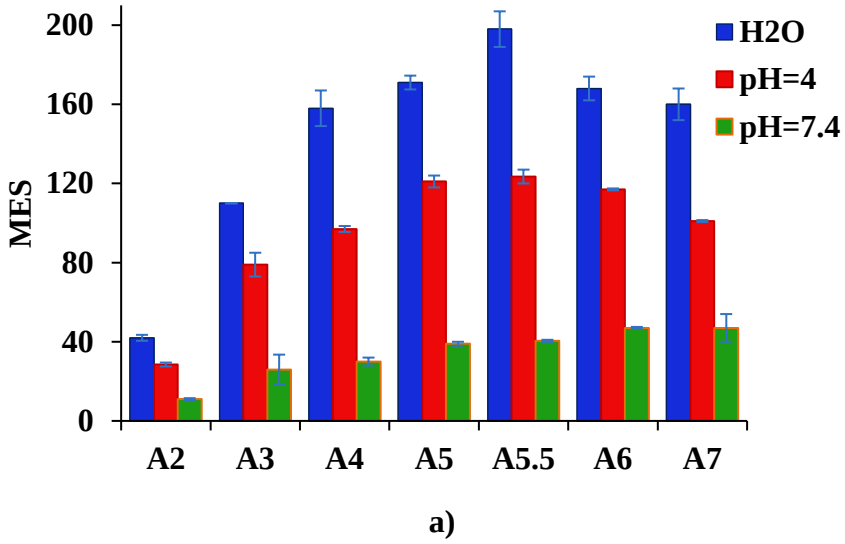

a)

c)

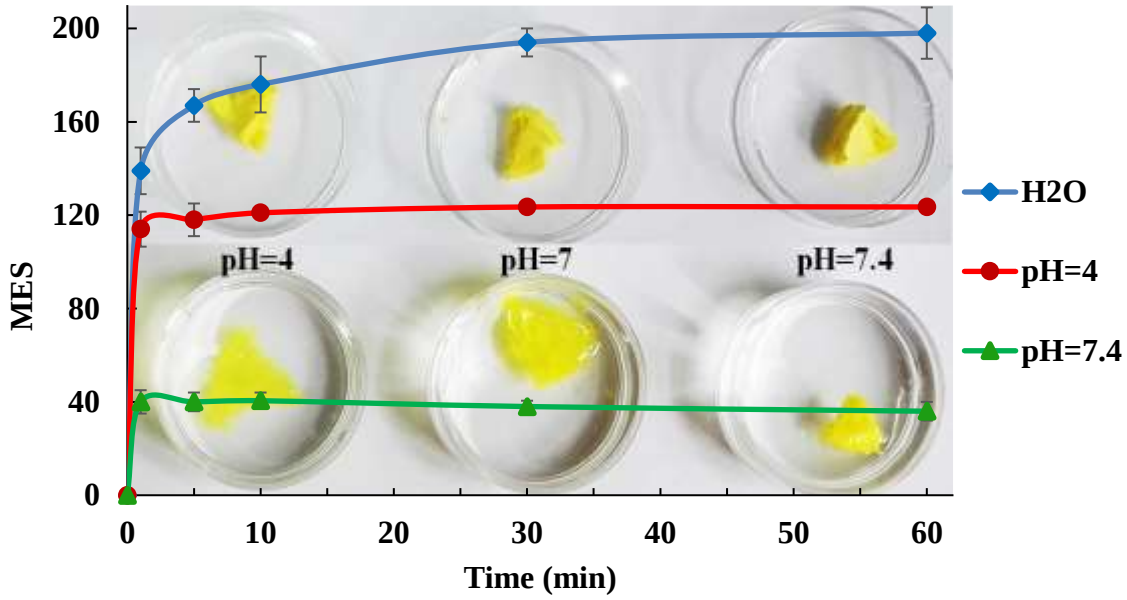

b)

Figure 4. Mass equilibrium swelling in different pH media of the **a)** hydrogels and **b) A5.5** measured during the time and hydrogel images before and after swelling in the three media; **c) A5.5** hydrogel injected in PBS

To monitor the hydrogel stability after swelling in different pH media, the FTIR spectra of the samples obtained by lyophilization of the hydrogels swollen for 3 months were registered. They showed slight less intense imine band compared to the FTIR spectra of the initial hydrogels, indicating a slow degradation (Supporting Information, Figure S4).

3.5.Rheology

To confirm the gel-like behaviour of the studied samples and to establish their mechanical properties, rheological behaviour of the samples was monitored by amplitude, frequency sweep and steady flow measurements and oscillatory step tests.

The linear viscoelastic regime (LVR) was determined at an increasing of the stress from $8x10^{-3}$ Pa to $5x10^{2}$ Pa, at a constant oscillation frequency of 10 rad/s (Figure 5a). The samples with NH_2/CHO ratio lower than 7 (**A4.5**-**A7**) had the G' elastic modulus higher than G" viscous modulus indicating a gel-like behaviour (Supporting Information, Table S1). On contrary, for the samples obtained with lower amount of nitrosalicylaldehyde (**A8.5**, **A10**) the G' elastic modulus overturned under the G" viscous one (G'<G"), in concordance with a liquid-like character. Viscoelastic parameters were constant for each sample up to a limiting shear stress (τ_L) value from which the structure began to change (Supporting Information, Table S1). The hydrogels with higher crosslinking density (**A4.5**, **A5**, **A5.5**) were stable up to about 150 Pa when the gel network started to destruct and the samples acquired liquid-like properties (Supporting Information, Table S1). Lower crosslinking densities determined lower τ_L values; the sample **A7** was stable up to 134 Pa, while the samples with NH_2/CHO ratio higher of 8.5 (**A8.5**, **A10**) showed significant lower values of τ_L around 25 Pa. Crosslinking of chitosan with a lower amount of nitrosalicylaldehyde induced a narrower LVR, in concordance with a lower density of imine linkages and thus lower density of crosslinking nodes. The elastic moduli vary as function of the NH_2/CHO ratio.

The gel properties of the **A4.5**-**A7** samples were further confirmed by the frequency sweep tests. As can be seen in figure 5b, their G', G'' rheological parameters increased as the density of the crosslinking nodes increased. The gel point has been accurately established by the calculation of the loss factor, tan δ, as ratio between the loss and storage moduli. It is generally accepted that tanδ > 1 indicates liquid-like properties, tan δ < 1 means gel-like behaviour, and the point at which tan δ becomes equal to unity (G' = G") represents the liquid-gel transition point. As can be seen in Supporting Information, Figure S5a, when tan δ was graphically represented as a function of the value of the NH_2/CHO ratio of the investigated samples, the gelling point has been reached for a NH_2/CHO ratio around 7.7.

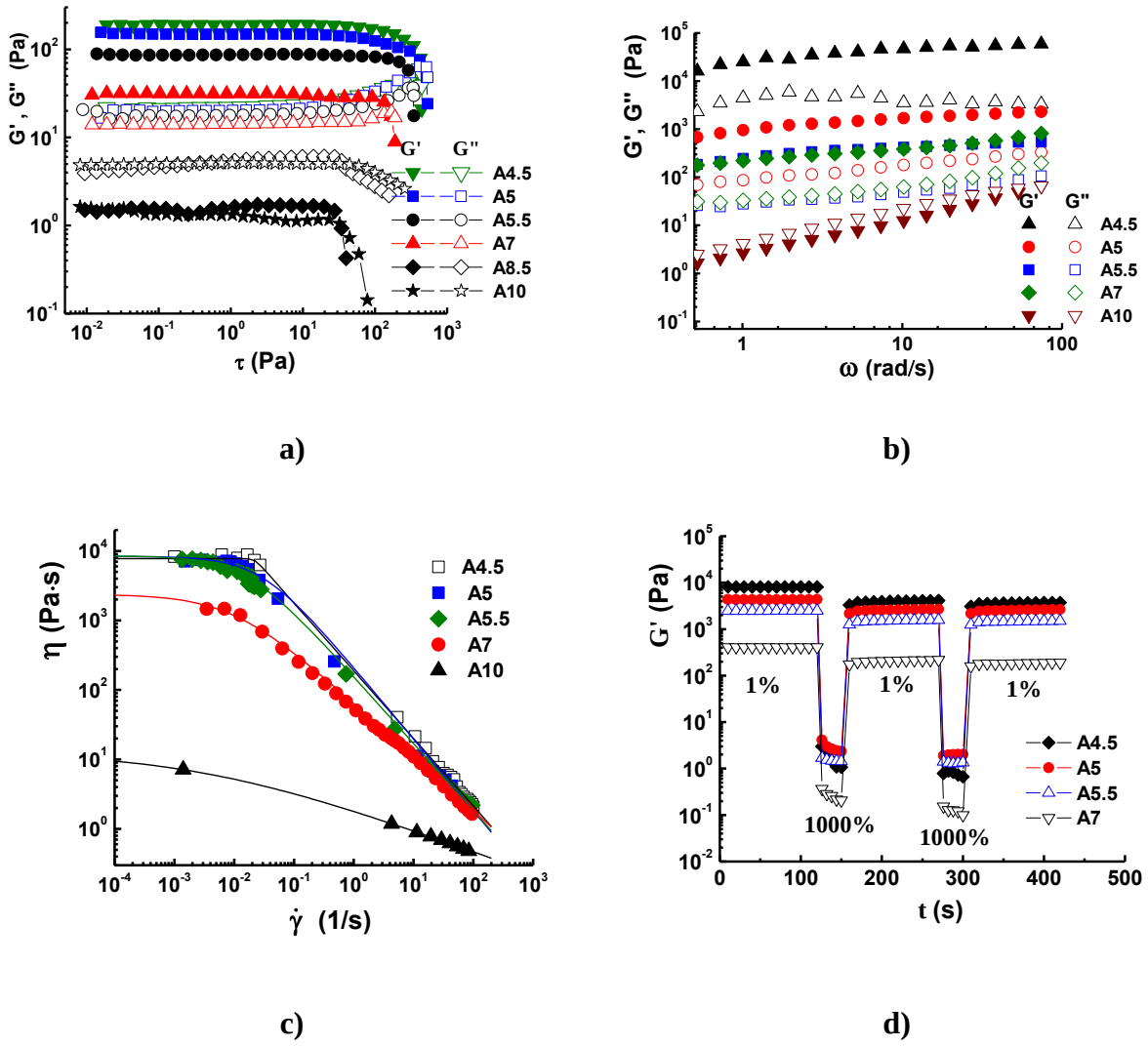

Figure 5. Rheological behaviour of the studied samples: a) Viscoelastic response as a function of applied shear stress at 10 rad/s and 37 °C; b) Frequency sweep determined at 1 rad/s and 37 °C; c) Flow curves (the full lines represent the fits of experimental data with Cross equation (eq. 1)); and d) Variation of G' and G" when the strain is alternating from 1% to 1000% at constant frequency (10 rad/s)

To establish the behaviour of the hydrogels under continuous flow, the steady shear experiments were performed at 37 °C, in the shear rate range between 10^{-3} 1/s - 10^{2} 1/s. All samples exhibited shear thinning behaviour and those in gel state presented yield stress (Figure 5c). The hydrogel samples revealed a critical value of the shear stress (yield stress, τ_c) at which the viscosity suddenly decreased and the hydrogels started to flow. As expected, the τ_c values goes to lower values as the crosslinking density of the samples

decreased (Supporting Information, Table S1), indicating more elastic hydrogels for a higher crosslinking density.

The value of zero shear viscosity (η_o) determined by using the Cross equation (Cross, 1965) remained almost constant for the samples with higher crosslinking density (**A4.5**, **A5**, **A5.5**) and abruptly decreased in the case of the samples **A7 - A10**, indicating the diminishing of the resistance to permanent deformations as the structure stiffness associated with crosslinking density decreased (Supporting Information, Figure S5b, Table S1) (Tamesue et al., 2013). A similar conclusion has been drawn looking to the values of α constant in Cross equation. Usually, high values of α are obtained for materials with structural breakdown at relatively low shear rate. As expected, the hydrogels characterized by high crosslinking density (**A4.5**, **A5**, **A5.5**) exhibited lower values of α indicating that their structural breakdown occurs at higher shear rate.

An important rheological parameter for hydrogels application is the recovery capacity of their mechanical properties (Zhu et al., 2017). The recovery for the hydrogel samples was investigated at 10 rad/s, in five consecutive steps, in which the strain is alternately changed from low strain (corresponding to LVR 1% for 120 s) to very high strain, above the deformation limit (1000% for 30 s). As can be seen in figure 5d, under low strain the hydrogels preserved their gel-like behaviour (G' > G"). Applying a high strain for a short period, G' and G" instantly decreased and G' became lower than G'' (G' < G") characteristic to the liquid-like samples, indicating the breaking of the hydrogel network. Upon the removal of the first high strain pulse the gel network recovered up to 50.7% - 60.4% of its initial structure (Supporting Information, Table S1). The structural recovery after the next high strain pulse was above 85% for all studied samples. The ability of the hydrogels to recover their mechanical properties after applying a high strain was not significantly influenced by the density of the imine covalent bonds and thus the crosslinking density. Generally speaking, the recovered strain degree and the viscoelastic parameters of the hydrogels based on chitosan are influenced by the nature of the crosslinking, physical or chemical one (Bercea, Bibire, Morariu, Teodorescu, & Carja, 2015). The values of the elastic recovery degree after subjected to repeated deformations were similarly to those reported for physical hydrogels based on chitosan, poly(ethylene oxide) and clay (Morariu, Bercea, & Sacarescu, 2014). The results are in agreement with the supramolecular architecture of the network nodes, in which the cohesion forces can be disrupted under a high strain and partial recovered during the low strain step.

3.6. Cytotoxicity tests

Literature survey revealed that some imines bearing nitrosalicylaldehyde residue exhibited antitumor activity (Luo, Sui, Lin, & Wu, 2016; Lu, Guo, Sang, & Guo, 2013; Zahedifard et al., 2015; Rama, & Selvameena, 2015). To evaluate the potential of the studied hydrogels in cancer therapy, their cytotoxicity against HeLa – a common human cancer cell-line, was investigated by MTS assay. To properly attribute the inhibitory activity, HeLa cells were incubated with hydrogels of different content of imine units (**A2** (0.318 µmol), **A3** (0.241 µmol), **A4 (**0.190 µmol)) and with equivalent molar amounts of model compound (**MC2** (0.318 µmol), **MC3** (0.241 µmol), **MC4** (0.190 µmol)) and aldehyde precursor (**NSA2** (0.318 µmol), **NSA3** (0.241 µmol), **NSA4** (0.190 µmol)).

As can be seen in figure 6, the model compound was the most active reducing the HeLa cells viability around 90 %, compared to the aldehyde precursor which diminished it more than 80 %. The higher activity of the model compound was attributed to the imine units and to the presence of glucosamine residue, as it was demonstrated that chitooligosaccharides inhibit the growth of tumour cells through an increase of immune effect (Xia, Liu, Zhang, & Chen, 2011). The hydrogels suppressed the HeLa cell viability around 60 %, after 48 hours. Their lower activity compared to the model compound and the precursor aldehyde can be assigned to the low mobility of the imine units linked on the chitosan chains which assure a prolonged killing effect. This hypothesis was confirmed by the bright-field microscopy images acquired after 24 and 48 hours, which clearly revealed a decrease of the living cell percentage in time (Figure 6f, g). A dose-dependent decrease pattern in HeLa cell viability was observed for the aldehyde and model compound, they being more effective at higher concentrations, when compared to corresponding negative control cells. More bright-field microscopy images were given in Supporting Information, Figure S6.

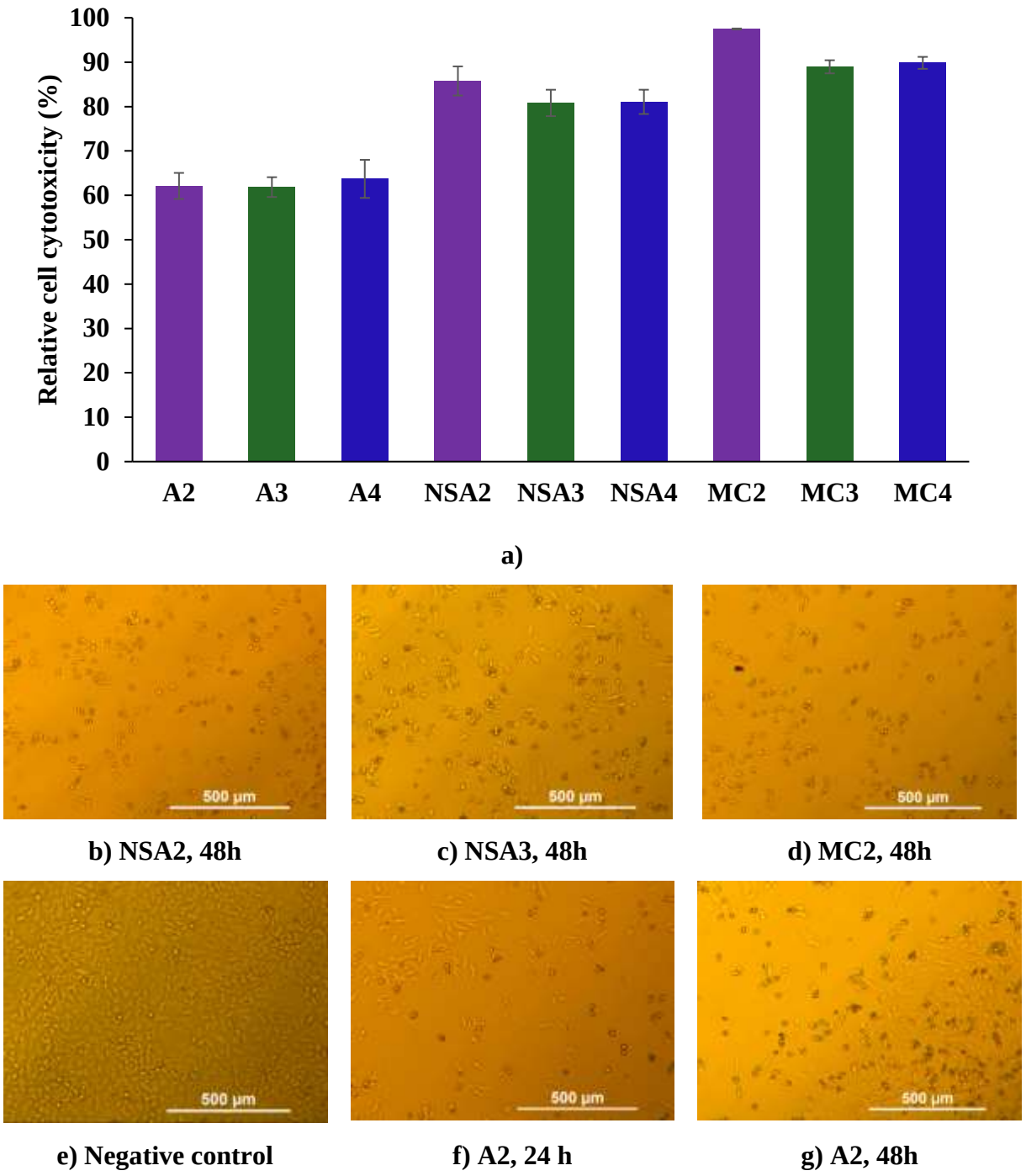

Figure 6. a) Cytotoxicity by MTS assays after 48 hours incubation of HeLa cells, at 37 ºC, with hydrogels of different molar content of imines (**A2** (0.318 µmol), **A3** (0.241 µmol), **A4** (0.190 µmol)) and with equivalent molar amounts of model compound (**MC2** (0.318 µmol), **MC3** (0.241 µmol), **MC4** (0.190 µmol)) and aldehyde precursor (**NSA2** (0.318 µmol), **NSA3** (0.241 µmol), **NSA4** (0.190 µmol)); Bright-field microscopy images of HeLa cells b)-d), f)-g) incubated with the studied samples for 24 or 48 hours and e) untreated HeLa cells

3.7. *In vivo* biocompatibility

In view of applying the studied hydrogels for local treatments, their biocompatibility has been investigated by measuring blood, biochemical and immune system parameters after

their subcutaneous administration in rats. As positive control reference, sterile cotton pellets saturated with saline solution were subcutaneous implanted in the control group (**C-p**), in order to create a standardized granuloma model, and a similar *in vivo* state for hydrogel-conditioned substances subcutaneous absorption (Peacman, 2011). A control group without implanted pellets were used as negative control reference (**C**).

In control rats with granuloma induced by sterile cotton pellets (**C-p**), it was shown a statistically significant (*p<0,05) increase in the percentage of polymorphonuclear neutrophils (PMN) and a statistically significant (*p<0,05) decrease in the percentage of peripheral blood lymphocites (Ly), compared to the control group without pellets (C), because of the local inflammatory reaction at the implantation site (Figure 7a, Supporting Information, Table S2). It was also observed a slightly increase in the monocytes (M) percentage, but statistically insignificant comparing with the control group without pellets (Figure 7c, Table 3s). On the contrary, the subcutaneous application of **A2**, **A3** and **A4** hydrogels caused an irrelevant increase of the PMN percentage and no essential differences of the Ly compared to the **C** control group without granuloma (Figure 7a,b, Supporting Information, Table S2). Also, no statistically significant modifications of the percentage of basophils and eosinophils in the animals with **A2**, **A3** and **A4** hydrogel implants was observed comparing with the control groups with or without pellets (Supporting Information, Table S2). The absence of a notable variation of the differential white cell percentage in the **A2**, **A3**, **A4** groups compared to the control (**C**) suggested that no infections, inflammations or autoimmune disease were induced by the subcutaneous implantation. An important role for this should be played by the ability of the chitosan to accelerate wound healing by enhancing the functions of inflammatory and repairing cells played (Sandri et al., 2017; Xia, Liu, Zhang, & Chen, 2011).

To see if the subcutaneous implantation of the hydrogels affected the biochemical activity, the plasmatic values of the metabolic key liver enzymes: glutamic pyruvic transaminase (GPT), glutamic oxaloacetic transaminase (GOT) and lactic dehydrogenase (LDH) were laboratory investigated. As can be seen in figure 7d, e, f, no major modifications of their activity in serum was observed, indicating no changes of the metabolic functions or structural damages of the tissue level of the **A2**, **A3** and **A4** groups compared to both control groups (**C**, **C-p**). The normal liver function was not affected by the hydrogel implantation, which had no noticeable toxicity effects.

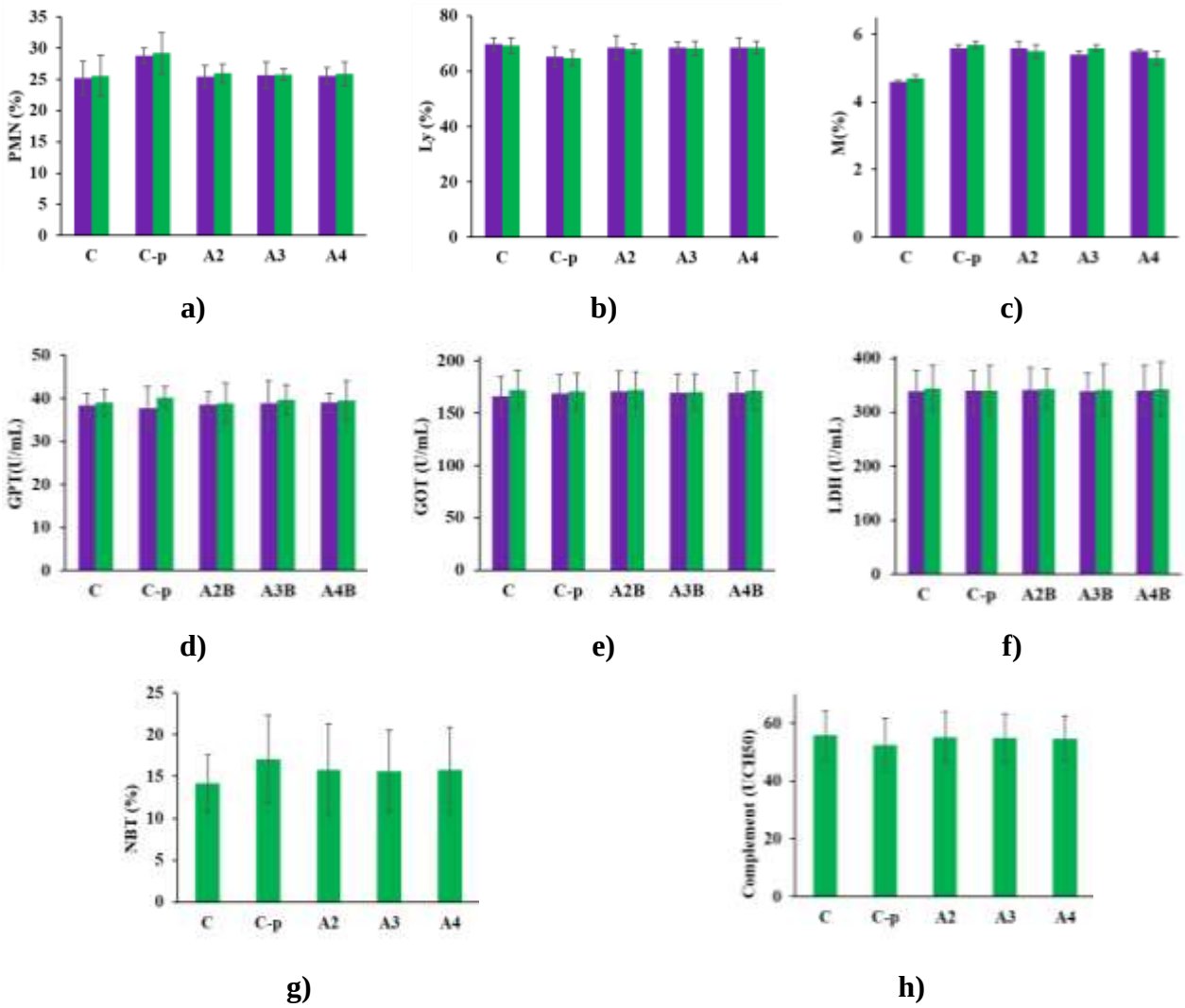

Figure 7. Variation of the **a**, **b**, **c**) differential white cell percentage (PMN, Ly, M), **d**, **e**, **f**) liver enzymes (GPT, GOT and LDH) activity and **g**, **h**) immune parameters NBT, Complement (UCH50), after subcutaneous implantation of the **A2**, **A3** and **A4** hydrogels in rats compared to the positive and negative control groups. Values were expressed as mean +/- standard deviation (SD) for 6 animals in a group (■: 24 hours; ■: 8 days)

Further, to investigate the immune system activity after implantation of the hydrogels, phagocytic capacity of peripheral blood (NBT) and serum complement activity (Complement (UCH50)) were determined. The results were given in Figure 7g, h. In the animals with experimental granuloma induced by cotton pellet implantation (**C-p**), it was observed a statistically significant (*****p<0,05) increase of phagocytic capacity of peripheral blood (NBT), compared to the control group without granuloma (**C**) due to the local inflammatory reaction (Supporting Information, Table S4). On the contrary, in the **A2**, **A3** and **A4** groups only a minor increase of the NBT was observed, statistically non-significant compared to the control

group without granuloma **(C)**. Minor influences were also registered for the serum complement activity (Complement **UCH50**), too. The induction of the experimental granuloma with sterile cotton pellets was associated with a statistically significant decrease (*****$p<0,05$) of serum complement activity compared to the control group without pellets, while the implantation of **A2**, **A3** and **A4** hydrogels resulted only in a slight diminishing, statistically non-significant compared to the control group without pellets (Supporting Information, Table S4). The negligible changes of these parameters indicate that the immune system activity was not affected by implantation of the studied hydrogels, which were not perceived as dangerous. This can be attributed to the influence of the chitosan, demonstrated to be having an immune stimulating activity (Liu, & Li, 2013).

The investigation of the effects on the blood, the serum biochemical and immune parameters revealed that the studied hydrogels presented good *in vivo* biocompatibility by administration as subcutaneous implants in rats, after 24 hours and 8 days, encouraging their use for local therapy.

CONCLUSIONS

A series of hydrogels based on chitosan and nitrosalicyladehyde have been prepared and their hydrogelation ability, rheological properties, *in vitro* cytotoxicity and *in vivo* biocompatibility were investigated. The hydrogelation occurred for a large range of the amine/aldehyde ratio, from 1/1 to 7.7/1, at different gelling times, allowing a large modulation of their properties. The hydrogelation was accelerated under physiological conditions (PBS, 37 ^{o}C), and the hydrogels presented self-healing in citrate buffer. They have superporous morphology and high mass equilibrium swelling in water and acidic buffer and a low MES with a good dimensional preservation in basic buffer at tissue pH. Rheological investigations revealed elastic hydrogels with good resistance to permanent deformations and good recovery of their mechanical properties. Incubation of HeLa cells with the studied hydrogels indicated *in vivo* cytotoxicity of 60 %, while the *in vivo* biocompatibility tested by subcutaneous administration in rats demonstrated insignificant changes of the blood, biochemical and immune system parameters. Entirely, all these measurements show that the novel synthesised hydrogels are promising biomaterials for implementation in local antitumor therapy, as drugs and matrixes for drug release.

ACKNOWLEDGEMENTS

This publication is part of a project that has received funding from the European Union's Horizon 2020 research and innovation programme under grant agreement 667387. The funding from the Romanian National Authority for Scientific Research, MEN – UEFISCDI grant, project number PN-II-RU-TE-2014-4-2314 is also acknowledged.

The authors are thankful to Professor Mihai Barboiu, Institut Européen des Membranes, Montpellier, France for useful discussions related to the reversibility of the imine linkage on chitosan.

REFERENCES

Ailincai, D., Marin, L., Morariu, S., Mares, M., Bostanaru, A. C., Pinteala, M., Simionescu, B. C., & Barboiu, M. (2016). Dual crosslinked iminoboronate-chitosan hydrogels with strong antifungal activity against Candida planktonic yeasts and biofilms. *Carbohydrate Polymers*, *152*, 306–316.

Beauchamp, R. O., St Clair, M. B. G., Fennell, T. R., Clarke, D. O., & Morgan, K. T. (1992). A critical review of the toxicology of glutaraldehyde. *Critical Reviews in Toxicology*, *22*, 143–174.

Bercea, M., Bibire, E.-L., Morariu, S., Teodorescu, M., & Carja, G. (2015). pH influence on rheological and structural properties of chitosan/poly(vinyl alcohol)/layered double hydroxide composites. *European Polymer Journal*, *70*, 147–156.

Chen, J., Park, H., & Park, K. (1999). Synthesis of superporous hydrogels: Hydrogels with fast swelling and superabsorbent properties. *Journal of Biomedical Materials Research*, *44*, 53–62.

Cross, M. M. (1965). Rheology of non-Newtonian fluids: A new flow equation for pseudoplastic systems. *Journal of Colloid Interface Science*, *20*, 417–437.

Dai, Z., Ronholm, J., Tian, T., Sethi, B., & Cao, X. (2016). Sterilization techniques for biodegradable scaffolds in tissue engineering applications. *Journal of Tissue Engineering*, 7, 1–13.

de Araújoa, E. L., Barbosa, H. F., Dockal, E. R., & Cavalheiro, É. T. (2017). Synthesis, characterization and biological activity of Cu(II), Ni(II) and Zn(II) complexes of biopolymeric Schiff bases of salicylaldehydes and chitosan. *International Journal of Biological Macromolecules*, *95*, 168–176.

De Jong, W. H., Carraway, J. W., & Geertsma, R. E. (2012). Biocompatibility and Performance of Medical Devices. In J.-P. Boutrand (Eds), *In vivo and in vitro testing for the biological safety evaluation of biomaterials and medical devices (pp. 120-158)*. Woodhead Publishing.

dos Santos, J. E., Dockal, E. R., & Cavalheiro, E. T. G. (2005). Synthesis and characterization of Schiff bases from chitosan and salicylaldehyde derivatives. *Carbohydrate Polymers, 60*, 277–282.

El-Sherbiny, I. M., & Yacoub, M. H. (2013). Hydrogel scaffolds for tissue engineering: Progress and challenges. *Global Cardiology Science & Practice, 3*, 316–342.

Ferreiraa, D.P.**,** Conceic¸ D.S.**,** Calhelhac, R.C.**,** Sousaa, T.**,** Socoteanub, R.**,** Ferreirac, I.C.F.R., & Vieira Ferreiraa, L.F. (2016). Porphyrin dye into biopolymeric chitosan films for localized photodynamic therapy of cancer. *Carbohydrate Polymers**, 151*, 160–171.

Geng, J., Zhao, X., Zhou, E., Li, G., Lam, J. W. Y., & Tang, B. Z. (2003). Shear induced molecular alignments of a side-chain liquid crystalline polyacetylene containing biphenyl mesogens. *Polymer, 44*, 8095–8102 .

Godoy-Alcántar, C., Yatsimirsky, A. K., & Lehn, J. -M. (2005). Structure-stability correlations for imine formation in aqueous solution. *Journal of Physical Organic Chemistry, 18*, 979–985.

Hoare, T. R., & Kohane, D. S. (2008). Hydrogels in drug delivery: Progress and challenges. *Polymer, 49*, 1993–2007

Hong, S. -C., Yoo, S. -Y., Kim, H., & Lee, J. (2017). Chitosan-Based Multifunctional Platforms for Local Delivery of Therapeutics. *Marine Drugs, 15*, 60.

Iftime, M., Morariu, S., & Marin, L. (2017). Salicyl-imine-chitosan hydrogels: Supramolecular architecturing as a crosslinking method toward multifunctional hydrogels. *Carbohydrate Polymers, 165*, 39–50.

Johnson, N. R., Kruger, M., Goetsch, K. P., Zilla, P., Bezuidenhout, D., Wang, Y., & Davies, N. H. (2015). Coacervate delivery of growth factors combined with a degradable hydrogel preserves heart function after myocardial infarction. *ACS Biomaterials Science & Engineering, 1*, 753–759.

Konieczynska, M. D., Villa-Camacho, J. C., Ghobril, C., Perez-Viloria, M., Tevis, K. M., Blessing, W. A., Nazarian, A., Rodriguez, E. K., & Grinstaf, M. W. (2016). On-demand dissolution of a dendritic hydrogel-based dressing for second-degree burn wounds through thiol–thioester exchange reaction. *Angewandte Chemie, 128*, 1–5.

Konieczynska, M. D., Villa-Camacho, J. C., Ghobril, C., Perez-Viloria, M., Blessing, W. A., Nazarian, A., Rodriguezb, E. K., & Grinstaffa, M. W. (2017). A hydrogel sealant for the treatment of severe hepatic and aortic trauma with a dissolution feature for post-emergent care. *Materials Horizons, 4*, 222–227.

Korupalli, C., Huang, C. -C., Lin, W. -C., Pan, W. -Y., Lin, P. -Y., Wan, W. -L., Li, M. -J., Chang, Y., & Sung, H. -W. (2017). Acidity-triggered charge-convertible nanoparticles that can cause bacterium-specific aggregation in situ to enhance photothermal ablation of focal infection. *Biomaterials, 116*, 1–9.

Kovaricek, P., & Lehn, J. M. (2012). Merging constitutional and motional covalent dynamics in reversible imine formation and exchange processes. *Journal of American Chemical Society, 134*, 9446–9455.

Latxague, L., Ramin, M. A., Appavoo, A., Berto, P., Maisani, M., Ehret, C., Chassande, O., & Barthelemy, P. (2015). Control of stem-cell behavior by fine tuning the supramolecular assemblies of low-molecular-weight gelators. *Angewandte Chemie- International Edition, 54*, 4517–4521.

Leceta, I., Guerrero, P., Ibarburu, I., Dueñas, M. T., & de la Caba, K. (2013). Characterization and antimicrobial analysis of chitosan-based films. *Journal of Food Engineering, 116*, 889–899.

Liu, Y., & Li, Z. -T. (2013). A dynamic route to structure and function: Recent advances in imine-based organic nanostructured materials. *Australian Journal of Chemistry, 66*, 9–22.

Lu, J., Guo, J., Sang, W., & Guo, H. (2013). Mixed-ligand oxovanadium complexes incorporating Schiff baseligands: synthesis, DNA interactions, and cytotoxicities. *Transition Metal Chemistry, 38*, 481–488.

Luo, H., Sui, Y., Lin, W. -H., & Wu, H. -Q. (2016). Study on the antiproliferative activity of four Schiff bases derived from natural biomass dehydroabietylamine. *Indian Journal of Chemistry, 55B*, 248–251.

Marin, L., Ailincai, D., Calin, M., Stan, D., Constantinescu, C. A., Ursu, L., Doroftei, F., Pinteala, M., Simionescu, B. C., & Barboiu, M. (2016). Dynameric frameworks for DNA transfection. *ACS Biomaterials Science & Engineering, 2*, 104–111.

Marin, L., Ailincai, D., Mares, M., Paslaru, E., Cristea, M., Nica, V., & Simionescu, B.C. (2015). Imino-Chitosan Biopolymeric Films. Obtaining, Self-assembling, Surface and Antimicrobial Properties. *Carbohydrate Polymers, 117*, 762–770.

723 Marin, L., Ailincai, D., Morariu, S., & Tartau-Mititelu, L. (2017). Development of
724 biocompatible glycodynameric hydrogels joining two natural motifs by dynamic
725 constitutional chemistry. *Carbohydrate Polymers, 170*, 60–71.
726 Marin, L., Morariu, S., Popescu, M. -C., Nicolescu, A., Zgardan, C., Simionescu, B. C., &
727 Barboiu, M. (2014). Out-of-water constitutional self-organization of chitosan–
728 cinnamaldehyde dynagels. *Chemistry A European Journal, 20*, 4814–4821.
729 Marin, L., Simionescu, B. C., & Barboiu, M. (2012). Imino-chitosan biodynamers. *Chemical*
730 *Communications, 48*, 8778–8780.
731 Mattaveewonga, T., Wongkrasant, P., Chanchai, S., Pichyangkurac, R., Chatsudthiponga, V.,
732 Muanprasat, C. (2016). Chitosan oligosaccharide suppresses tumor progression in a mouse
733 model of colitis-associated colorectal cancer through AMPK activation and suppression of
734 NF-B and mTOR signalling. *Carbohydrate Polymers*, *145*, 30–36.
735 Montembault, A., Viton, C., & Domard, A. (2005). Rheometric study of the gelation of
736 chitosan in aqueous solution without cross-linking agent. *Biomacromolecules, 6*, 653–662.
737 Morariu, S., Bercea, M., & Sacarescu, L. (2014). Tailoring of clay/poly(ethylene oxide)
738 hydrogel properties by chitosan incorporation. *Industrial & Engineering Chemistry*
739 *Research, 53*, 13690–13698.
740 Naderi-Meshkin, H., Matin, M. M., Heirani-Tabasi, A., Mirahmadi, M., Irfan-Maqsood, M.,
741 Edalatmanesh, M. A., Shahriyari, M., Ahmadiankia, N., Moussavi, N. S., Bidkhori, H. R.,
742 & Bahrami, A. R. (2016). Injectable hydrogel delivery plus preconditioning of
743 mesenchymal stem cells: exploitation of SDF-1/CXCR4 axis toward enhancing the
744 efficacy of stem cells' homing. *Cell Biology International, 40*, 730–741.
745 Nasr, G., Petit, E., Vullo, D., Winum, J. -Y., Supuran, C. T., & Barboiu, M. (2009). Carbonic
746 anhydrase-encoded dynamic constitutional libraries: Toward the discovery of isozyme-
747 specific inhibitors. *Journal of Medicinal Chemistry, 52*, 4853–4859.
748 Peacman M., (2011). Clinical & Experimental Immunology, British Society of Immunology,
749 Wiley Library.
750 Pestova, A. V., Mehaeva, A. V., Kodess, M. I., Ezhikova, M. A., Azarova, Y. A., & Bratskay,
751 S. Y. (2016). Imidazolyl derivative of chitosan with high substitution degree: Synthesis,
752 characterization and sorption properties. *Carbohydrate Polymers, 138*, 252–258.
753 Protocole d'amendement à la convention européenne sur la protection des animaux vertébrés
754 utilisés à des fins expérimentales ou à d'autres fins scientifiques. Strasbourg; 22.06.1998.

Punnia-Moorthy, A. (1987). Evaluation of pH changes in inflammation of the subcutaneous air pouch lining in the rat, induced by carrageenan, dextran and staphylococcus aureus. *Journal of Oral Pathology & Medicine, 16*, 36–44.

Rama, I., & Selvameena, R. (2015). Synthesis, structure analysis, anti-bacterial and in vitro anti-cancer activity of new Schiff base and its copper complex derived from sulfamethoxazole. *Journal of Chemical Science, 127*, 671–678.

Ruff, Y., Buhler, E., Candau, S. -J., Kesselman, E., Talmon, Y., & Lehn, J. -M. (2010). Glycodynamers: Dynamic polymers bearing oligosaccharides residues - Generation, structure, physicochemical, component exchange, and lectin binding properties. *Journal of the American Chemical Society, 132*, 2573–2584.

Salis, A., Rassu, G., Budai-Szücs, M., Benzoni, I., Csányi, E., Berkó, S., Maestri, M., Dionigi, P., Porcu, E. P., Gavini, E., & Giunched, P. (2015). Development of thermosensitive chitosan/glicerophospate injectable in situ gelling solutions for potential application in intraoperative fluorescence imaging and local therapy of hepatocellular carcinoma: a preliminary study. *Expert Opinion Drug Delivery, 12*, 1583–1596.

Sandri, G., Aguzzi, C., Rossi, S., Bonferoni, M. C., Bruni, G., Boselli, C., Cornaglia, A. I., Riva, F., Viseras, C., Caramella, C., & Ferrari, F. (2017). Halloysite and chitosan oligosaccharide nanocomposite for wound healing. *Acta Biomaterialia, 57*, 216–224.

Sedghi, R., Shaabani, A., Mohammadi, Z., Samadi, Z. Y., & Isae, F. (2017). Biocompatible electrospinning chitosan nanofibers: A novel delivery system with superior local cancer therapy. *Carbohydrate Polymers, 159*, 1–10.

Storrie, H., Guler, M. O., Abu-Amara, S. N., Volberg, T., Rao, M., Geiger, B., & Stupp, S. I. (2007). Supramolecular crafting of cell adhesion. *Biomaterials, 28*, 4608–4618.

Stroescu, M., Stoica-Guzun, A., Isopencu, G., Jinga, S. I., Parvulescu, O., Dobre, T., & Vasilescu, M.. (2015). Chitosan-vanillin composites with antimicrobial properties. *Food Hydrocolloids, 48*, 62–71.

Ta H. T., Dass C. R., & Dunstan D. E., (2008). Injectable chitosan hydrogels for localised cancer therapy. *Journal of Controlled Release, 126*, 205–216.

Tamesue, S., Ohtani, M., Yamada, K., Ishida, Y., Spruell, J. M., Lynd, N. A., Hawker, C. J., & Aida, T. (2013). Linear versus dendritic molecular binders for hydrogel network formation with clay nanosheets: Studies with ABA triblock copolyethers carrying guanidinium ion pendants. *Journal of American Chemical Society, 135*, 15650–15655.

Wang, M.O., Etheridge, J.M., Thompson, J.A., Vorwald, C.E., Dean, D. & Fisher, J.P. (2013). Evaluation of the In Vitro Cytotoxicity of Cross-Linked Biomaterials. *Biomacromolecules*, 14, 1321−1329.

Wolf, M. F., & Andwraon, J. M. (2012). Biocompatibility and Performance of Medical Devices. In J.-P. Boutrand (Eds) *Practical approach to blood compatibility assessments: general considerations and standards (pp. 159-200).* Woodhead Publishing.

Xia, W., Liu, P., Zhang, J., & Chen, J. (2011). Biological activities of chitosan and chitooligosaccharides. *Food Hydrocolloids, 25*, 170–179.

Zabulica, A., Perju, E., Bruma, M., Marin, L. (2014). Novel luminescent liquid crystalline polyazomethines. Synthesis and study of thermotropic and photoluminescent properties, *Liquid Crystals, 41*, 252–262.

Zahedifard, M., Faraj, F. L., Paydar, M., Looi, C. Y., Hajrezaei, M., Hasanpourghadi, M., Kamalidehghan, B., Majid, N. A., Ali, H. M., & Ameen, M. (2015). Synthesis, characterization and apoptotic activity of quinazolinone Schiff base derivatives toward MCF-7 cells via intrinsic and extrinsic apoptosis pathways. *Scientific Reports, 5*, 11544.

Zhang, X., Lin, Y., & Gillies, R. J. (2010). Tumor pH and its measurement. *Journal of Nuclear Medicine, 51*, 1167–1170.

Zhu, S., Yu, X., Xiong, S., Liu, R., Gu, Z., You, J., Yin, T., & Hu, Y. (2017). Insights into the rheological behaviors evolution of alginate dialdehyde crosslinked collagen solutions evaluated by numerical models. *Materials Science and Engineering C, 78*, 727–737.

Graphical abstract